Expedited Machine-Learning-Based Global Design Optimization of Antenna Systems Using Response Features and Multi-Fidelity EM Analysis

Anna Pietrenko-Dabrowska[1[0000-0003-2319-6782]], Slawomir Koziel[2,1[0000-0002-9063-2647]], and Leifur Leifsson[3[0000-0001-5134-870X]]

[1] Faculty of Electronics Telecommunications and Informatics, Gdansk University of Technology, Narutowicza 11/12, 80-233 Gdansk, Poland
anna.dabrowska@pg.edu.pl
[2] Engineering Optimization & Modeling Center, Department of Engineering, Reykjavík University, Menntavegur 1, 102 Reykjavík, Iceland
koziel@ru.is
[3] School of Aeronautics and Astronautics, Purdue University, West Lafayette, IN 47907, USA
leifur@purdue.edu

Abstract. The design of antenna systems poses a significant challenge due to stringent performance requirements dictated by contemporary applications and the high computational costs associated with models, particularly full-wave electromagnetic (EM) analysis. Presently, EM simulation plays a crucial role in all design phases, encompassing topology development, parametric studies, and the final adjustment of antenna dimensions. The latter stage is especially critical as rigorous numerical optimization becomes essential for achieving optimal performance. In an increasing number of instances, global parameter tuning is necessary. Unfortunately, the use of nature-inspired algorithms, the prevalent choice for global design, is hindered by their poor computational efficiency. This article presents an innovative approach to cost-efficient global optimization of antenna input characteristics. Our methodology leverages response feature technology, ensuring inherent regularization of the optimization task by exploring the nearly-linear dependence between the coordinates of feature points and the antenna's dimensions. The optimization process is structured as a machine learning (ML) procedure, utilizing a kriging surrogate model rendering response features to generate promising candidate designs (infill points). This model is iteratively refined using accumulated EM simulation data. Further acceleration is achieved by incorporating multi-fidelity EM analysis, where initial sampling and surrogate model construction use low-fidelity EM simulations, and the ML optimization loop employs high-fidelity EM analysis. The multi-fidelity EM simulation data is blended into a single surrogate using co-kriging. Extensive verification of the presented algorithm demonstrates its remarkable computational efficiency, with an average running cost not exceeding ninety EM simulations per run and up to a seventy percent relative speedup over the single-fidelity procedure.

Keywords: Antenna design; global optimization; computer-aided design; response features; bio-inspired algorithms; variable-fidelity EM analysis.

ICCS Camera Ready Version 2024
To cite this paper please use the final published version:
DOI: 10.1007/978-3-031-63775-9_2

1 Introduction

The development of contemporary antennas presents considerable challenges. On one hand, stringent performance requirements, guided by both existing and emerging application areas [1]-[3], encompass a range of electrical and field parameters (among others, wideband and multi-band operation, high gain, circular polarization, beam scanning [4]-[6]), reconfigurability [7], and constraints related to small physical dimensions [8]. On the other hand, addressing the intricacies of antenna geometries crafted to meet these demands [9], [10] poses a substantial challenge on its own. Traditional parametric studies, often employed for dimension adjustments, are found lacking in the control of multiple variables, not to mention the consideration of various design objectives or constraints. As a more robust alternative, formal numerical optimization methods [11] are recommended. However, the accurate assessment of antenna responses necessitates full-wave electromagnetic (EM) analysis, a resource-intensive process. Given that EM-driven optimization often requires a large number of antenna simulations, the resulting computational expenses could be prohibitive. Even the costs associated with local parameter adjustment, whether gradient-based [12] or stencil-based [13], may be significant. Global [14] or multi-objective optimization [15], as well as uncertainty quantification [16], entail considerably higher expenses, with the usual number of objective function evaluations easily reaching several thousand.

Despite the challenges associated with global optimization, its significance in antenna design is on the rise. On one hand, there is a growing number of inherently multimodal problems, such as pattern synthesis of antenna arrays, design of frequency-selective surfaces, or the creation of metamaterials and metasurfaces [17]. On the other hand, many antenna structures incorporate various topological alterations, such as stubs, defected ground structures, and shorting pins [18], aiming to enhance antenna performance but also introducing parameter redundancy and expanding the search space [19]. Other reasons for employing global optimization methods include the need for antenna re-design across an extensive range of operating conditions (e.g., center frequencies) or the absence of an initial design of sufficient quality. Currently, global optimization is predominantly driven by bio-inspired population-based procedures [20], [21]. These algorithms process sets of candidate solutions for the given problem. Their global search capability is often attributed to information exchange among individuals in the population [22], and the utilization of partially-stochastic mechanisms such as selection and recombination [23]. Various bio-inspired algorithms, including genetic and evolutionary algorithms, particle swarm optimizers (PSO), firefly algorithm, or grey wolf optimization, are widely used [24]-[27]. However, new methods in this category are continually proposed [28], [29]. While population-based procedures are structurally simple and easy to handle, their computational efficiency is inferior. The typical running costs of a nature-inspired algorithm can reach several thousand objective function calls. Thus, their direct use in EM-driven design is essentially prohibitive. In practice, these algorithms are employed only when the underlying merit function is inexpensive to evaluate (especially if it is analytical or EM-based but takes less than ten seconds per simulation) or when parallelization is facilitated by available resources and licensing.

Enabling practical electromagnetic (EM)-driven optimization using bio-inspired algorithms becomes feasible through the application of surrogate modeling techniques

ICCS Camera Ready Version 2024
To cite this paper please use the final published version:
DOI: 10.1007/978-3-031-63775-9_2

[30]. A common configuration for a surrogate-assisted procedure involves utilizing the metamodel as a rapid predictor to generate candidate solutions, with iterative surrogate enhancement utilizing accumulated EM simulation data [31]. These candidate solutions, known as infill points, may be generated based on different criteria aiming to enhance model reliability (exploration), identify a globally-optimum design (exploitation), or strike a balance between exploitation and exploration [32]. The role of a bio-inspired search is to globally optimize the surrogate model or identify parameter space regions with the highest expected modeling error. The computational advantages arise from the fact that the majority of operations occur at the level of the fast metamodel rather than directly using EM analysis. Commonly utilized modeling techniques encompass kriging, Gaussian Process Regression (GPR), and neural networks [33], [34]. Optimization procedures following the discussed scheme are often referred to as machine learning (ML) frameworks [35]. Despite the advantages of surrogate-assisted methods, they face challenges related to the rendition of a dependable behavioral model. The complexity arises from the prononunced nonlinearity of antenna responses and the vast size of the search space. Typically, these procedures are demonstrated using relatively simple (especially low-dimensional) test cases [36]. Mitigation methods available in the literature include performance-driven modeling [37]; however, its integration into global search procedures is not straightforward. Other techniques include multi-fidelity EM simulations [38], and response feature technology [39], which proves useful for local tuning as well as surrogate modeling. Feature-based methods capitalize on re-stating the design problem with regard to carefully appointed characteristic points of the component outputs (in the case of antennas, usually, frequency and level values of their resonances) and leveraging nearly-linear dependence between these coordinates and original designable parameters (predominantly, geometry ones). Response features have been demonstrated to efficiently regularize the design task, resulting in faster convergence, and reducing the training dataset size necessary to construct a dependable behavioral model [40], [41].

The aim of this research is to present an innovative method for surrogate-based global optimization of antenna input characteristics. Our approach integrates a machine learning (ML) framework with kriging interpolation surrogates and multi-fidelity electromagnetic (EM) simulation models. In the initial phase of the search process, encompassing parameter space sampling and initial surrogate model construction, low-fidelity EM analysis is employed. Within the primary ML loop, the high-resolution model is used, and the model (predictor) generates candidate solutions (infill points) using the particle swarm optimizer (PSO) as the underlying search engine. The infill criterion is the minimization of the predicted objective function. The model is then refined with accumulated EM simulation data, and low- and high-fidelity data samples are merged into a single metamodel using co-kriging. The entire search process is conducted by re-stating the problem in terms of the response features of the antenna under consideration. Comprehensive verification studies demonstrate the remarkable computational efficiency of the proposed technique, with an average running cost not exceeding ninety high-fidelity EM simulations. This corresponds to a significant relative acceleration of up to seventy percent over various state-of-the-art benchmark methods, including both bio-inspired and ML algorithms. Simultaneously, our algorithm exhibits excellent reliability and repeatability of results.

ICCS Camera Ready Version 2024
To cite this paper please use the final published version:
DOI: 10.1007/978-3-031-63775-9_2

2 Global Optimization Using Response Features and Multi-Fidelity EM Analysis

This part of the paper outlines the developed optimization framework. We start by formulating the optimization problem in Section 2.1 with focus on multi-band antenna input characteristics. Section 2.2 reprises the notion of response features, whereas Section 2.3 is devoted to the variable-resolution EM simulations. Subsequent sections delineate kriging and co-kriging modelling (Section 2.4), which are employed for construction of a primary low-fidelity surrogate (Section 2.5), and high-fidelity model refinement (Section 2.6). Section 2.7 offers a summary of the entire procedure.

2.1 Antenna Design Task: Formulation

As we focus on optimization of the input characteristics of multi-band antennas, our aim is to arrange antenna resonances at specific locations, i.e., intended (target) frequencies $\boldsymbol{F}_t = [f_{t.1} \ \ldots \ f_{t.K}]^T$. We also strive to enhance the impedance matching at the same locations, which corresponds to minimization of the modulus of the reflection coefficient $|S_{11}|$ at $f_{t.j}$, $j = 1, \ldots, K$. This problem utilizes a minimax objective function. Table 1 provides the basic notation, using which the design task may be expressed as

$$\boldsymbol{x}^* = \arg\min_{\boldsymbol{x}} U(\boldsymbol{x}, \boldsymbol{F}_t) \tag{1}$$

Other design problems are also conceivable, such as maximization of the impedance bandwidth or antenna gain enhancement. Yet, the particular task discussed in this study may serve as an illustrative scenario frequently encountered in practical applications.

2.2 Concept of Response Features

The main hardship in EM-driven antenna design optimization is the significant cost of multiple EM analyses, inevitably invoked by numerical search process. This expenses are troublesome for local optimization and increase radically when global algorithms are at play. In the global search, the entire design space—vast both in terms of dimensionality and span—needs to be explored, which presents a challenging task. Nonlinearity of antenna outputs, particularly for multi-band antennas, add further complexity to this undertaking. Similarly, due to the response shape, rendition of a dependable surrogate accurately representing the characteristics of interest is intricate.

The response feature approach [42] can be employed for tackling the aforementioned difficulties. The response feature technology requires that the design task is redefined with regard to characteristic points of the antenna outputs. This allows to take the advantage of the nearly-linear dependency of the feature point coordinates (typically, frequencies and levels of characteristic locations in the frequency characteristics) on antenna dimensions [39]. Applying this method permits regularization of the merit function, and speeding up the convergence of the entire search. Additionally, quasi-global search capabilities are enabled [39], whereas the data set size for creating a dependable model is largely reduced [40]. It is of paramount importance that feature points coincide with the design goals [42]. For example, in the case of impedance matching improvement of multi-band structures, frequency and level locations pertinent to antenna resonances are particularly useful.

ICCS Camera Ready Version 2024
To cite this paper please use the final published version:
DOI: 10.1007/978-3-031-63775-9_2

Table 1. Multi-band antenna optimization: Basic notation

Symbol	Meaning	Comment
$\boldsymbol{x} = [x_1 \ldots x_n]^T$	Vector of antenna designable variables	Typically, antenna geometry parameters
$S_{11}(\boldsymbol{x},f)$	Antenna reflection at a given design $\boldsymbol{x}$ and frequency f	Reflection coefficient is a complex number; we handle its modulus $\lvert S_{11}\rvert$ [dB]
$F_t = [f_{t.1} \ldots f_{t.K}]^T$	Vector of target operating frequencies	Frequencies corresponding to the intended allocation of antenna resonances
$U(\boldsymbol{x},\boldsymbol{F}_t)$	Objective function (to be minimized by the search procedure)	Function quantifying the design quality, we use: $U(\boldsymbol{x},\boldsymbol{F}_t) = \max_x \{\lvert S_{11}(\boldsymbol{x},f_{t.1})\rvert,\ldots,\lvert S_{11}(\boldsymbol{x},f_{t.K})\rvert\}$

Let us define a response feature vector $\boldsymbol{f}_P(\boldsymbol{x}) = [\boldsymbol{f}_f(\boldsymbol{x})^T \boldsymbol{f}_L(\boldsymbol{x})^T]^T$, with $\boldsymbol{f}_f(\boldsymbol{x}) = [f_{f.1}(\boldsymbol{x}) \ldots f_{f.K}(\boldsymbol{x})]^T$ and $\boldsymbol{f}_L(\boldsymbol{x}) = [f_{L.1}(\boldsymbol{x}) \ldots f_{L.K}(\boldsymbol{x})]^T$ being its horizontal and vertical coordinates, respectively. The merit function may be expressed with regard to response features as

$$U_F(\boldsymbol{x}, \boldsymbol{f}_P, \boldsymbol{F}_t) = \max_{\boldsymbol{x}} \{f_{L.1}(\boldsymbol{x}),\ldots,f_{L.K}(\boldsymbol{x})\} + \beta \,\|\, \boldsymbol{f}_f - \boldsymbol{F}_t \,\|^2 \quad (2)$$

In (2), the second term $\beta \|\boldsymbol{f}_f - \boldsymbol{F}_t\|^2$ corresponds to a regularization factor, enforcing alignment of the resonant frequencies with their required allocations. The factor β should be set so as to guarantee that the regularization term sufficiently contributes when necessary (i.e., if resonances are largely misaligned (we have $\beta = 100$). Despite the fact that (2) differs from the minimax formulation of Table 1, yet, the respective optimum solutions coincide (provided they are reachable).

Table 2. Basic definitions of kriging and co-kriging modeling

Model	Component	Analytical form
Kriging	Model formulation	$\boldsymbol{s}_{KR}(\boldsymbol{x}) = \boldsymbol{M}\gamma + r(\boldsymbol{x})\cdot\boldsymbol{\Psi}^{-1}\cdot(\boldsymbol{R}_c(X_{Bc}) - \boldsymbol{F}\gamma)$ where: $\boldsymbol{M}$ – $N_{Bc} \times t$ model matrix of X_{Bc}, $\boldsymbol{F}$ – $1 \times t$ vector of the evaluation point $\boldsymbol{x}$, t –number of terms used in the regression function
	Regression function coefficients	$\gamma = ({X_{Bc}}^T \boldsymbol{\Psi}^{-1} X_{Bc})^{-1} X_{Bc} \boldsymbol{\Psi}^{-1} \boldsymbol{R}_f(X_{Bc})$
	Vector of correlations between $\boldsymbol{x}$ and X_{Bc}	$r(\boldsymbol{x}) = (\psi(\boldsymbol{x}, \boldsymbol{x}_{Bc}^{(1)}),\ldots,\psi(\boldsymbol{x}, \boldsymbol{x}_{Bc}^{(N_{Bc})}))$
	Correlation matrix	$\boldsymbol{\Psi} = [\Psi_{i,j}]$ is a correlation matrix, where $\Psi_{i,j} = \psi(\boldsymbol{x}_{Bf}^{(i)}, \boldsymbol{x}_{Bf}^{(j)})$
	Correlation function	$\psi(\boldsymbol{x}, \boldsymbol{x}') = \exp\left(\sum_{k=1}^{n} -\theta_k \mid x^k - x'^k \mid^P\right)$
	Model identification: finding hyperparameters θ_k, $k = 1, \ldots, n$, using Maximum Likelihood Estimation (MLE)	$(\theta_1,\ldots,\theta_n) = \arg\min_{\theta_1,\ldots,\theta_n}\left[-(N_{Bf}/2)\ln(\hat{\sigma}^2) - 0.5\ln(\lvert\Psi\rvert)\right]$ where $\hat{\sigma}^2 = (\boldsymbol{R}_f(X_{Bf}) - F\alpha)^T \boldsymbol{\Psi}^{-1}(\boldsymbol{R}_f(X_{Bf}) - F\alpha)/N_{Bf}$ and $\lvert\Psi\rvert$ is the determinant of $\boldsymbol{\Psi}$. In practice, a Gaussian correlation function ($P = 2$) is often employed, as well as $\boldsymbol{F} = [1 \ldots 1]^T$ and $\boldsymbol{M} = 1$.
Co-kriging	Model formulation	$\boldsymbol{s}_{CO}(\boldsymbol{x}) = \boldsymbol{M}\gamma + r(\boldsymbol{x})\cdot\boldsymbol{\Psi}^{-1}\cdot(\boldsymbol{r} - \boldsymbol{F}\gamma)$
	Vector of correlations	$r(\boldsymbol{x}) = [\rho\cdot\sigma_c^2\cdot r_c(\boldsymbol{x}), \rho^2\cdot\sigma_c^2\cdot r_c(\boldsymbol{x}, X_{B_f}) + \sigma_d^2\cdot r_d(\boldsymbol{x})]$
	Correlation matrix	$\boldsymbol{\Psi} = \begin{bmatrix} \sigma_c^2\boldsymbol{\Psi}_c(X_{Bc}, X_{Bc}) & \rho\,\sigma_c^2\boldsymbol{\Psi}_c(X_{Bc}, X_{Bf}) \\ \rho\,\sigma_c^2\boldsymbol{\Psi}_c(X_{Bf}, X_{Bc}) & \rho^2\sigma_c^2\boldsymbol{\Psi}_c(X_{Bf}, X_{Bf}) + \sigma_d^2\boldsymbol{\Psi}_d \end{bmatrix}$ where $\boldsymbol{M} = [\rho\boldsymbol{M}_c\, \boldsymbol{M}_d]$, whereas ($\boldsymbol{F}_c$, σ_c, $\boldsymbol{\Psi}_c$, $\boldsymbol{M}_c$) and ($\boldsymbol{F}_d$, σ_d, $\boldsymbol{\Psi}_d$, $\boldsymbol{M}_d$) are matrices obtained from $\boldsymbol{s}_{KRc}$ and $\boldsymbol{s}_{KRf}$, respectively; parameter ρ is included in the MLE during model identification.

ICCS Camera Ready Version 2024
To cite this paper please use the final published version:
DOI: 10.1007/978-3-031-63775-9_2

2.3 Multi-Resolution EM Simulations

Low-fidelity models can expedite design optimization procedures mainly by diminishing the time needed for system evaluation at the expense of deteriorating its accuracy. In antenna design, low-resolution models are realized as coarse-discretization EM models. Depending on the intricacy of the antenna topology, various levels of acceleration can be achieved. Typical speedup ranges from below three to over ten in some cases.

In this study, the role of the low-resolution surrogate, labelled as $\boldsymbol{R}_c(\boldsymbol{x})$, will be twofold: (i) rendition (random) of observable set utilized for design space pre-screening, and (ii) construction of the primary surrogate (in the form of a kriging interpolant, as explained in Section 2.4). As the procedure advances, co-kriging model will be employed for merging low- and high-fidelity points to establish an enhanced surrogate. We will use $\boldsymbol{R}_f(\boldsymbol{x})$ to represent the high-fidelity model.

2.4 Kriging and Co-Kriging Metamodels

Kriging and co-kriging models [38] are utilized in this study as predictors guiding optimization procedure towards global solution. We will use $\{\boldsymbol{x}_{Bc}^{(k)},\boldsymbol{R}_c(\boldsymbol{x}_{Bc}^{(k)})\}_{k=1,\ldots,NBc}$, to denote the low-fidelity dataset comprising designs $\boldsymbol{x}_{Bc}^{(k)}$ with relevant responses. Let also $\{\boldsymbol{x}_{Bf}^{(k)},\boldsymbol{R}_f(\boldsymbol{x}_{Bf}^{(k)})\}_{k=1,\ldots,NBf}$, represent the high-fidelity dataset, EM-evaluated at a high-fidelity resolution at the vectors $\boldsymbol{x}_{Bf}^{(k)}$.

Table 2 compiles the relevant notation as well as the details pertaining to kriging and co-kriging surrogates: $\boldsymbol{s}_{KR}(\boldsymbol{x})$ and $\boldsymbol{s}_{CO}(\boldsymbol{x})$, respectively. In general, co-kriging surrogate constitutes a composite of two models. The first one is a kriging model $\boldsymbol{s}_{KRc}$ whose training data set is of low-resolution, we have $(X_{Bc}, \boldsymbol{R}_c(X_{Bc}))$. Whereas the second model, $\boldsymbol{s}_{KRf}$, is established based on the residuals $(X_{Bf}, \boldsymbol{r})$, with $\boldsymbol{r} = \boldsymbol{R}_f(X_{Bf}) - \rho\cdot\boldsymbol{R}_c(X_{Bf})$, where ρ is derived by the Maximum Likelihood Estimation (MLE) of the second model [43]. Both $\boldsymbol{s}_{KR}(\boldsymbol{x})$ and $\boldsymbol{s}_{CO}(\boldsymbol{x})$ utilize the same correlation function, see Table 2.

2.5 Pre-Screening of Design Space. Primary Surrogate Construction

In our approach, the first stage of the search process consists in gathering an ensemble of random low-fidelity parameter vectors. Using the eligible samples (i.e., such whose frequency characteristics enable feature point extraction) the primary surrogate $\boldsymbol{s}^{(0)}(\boldsymbol{x})$ is established as a kriging interpolation metamodel [38].

$$\boldsymbol{s}^{(0)}(\boldsymbol{x}) = \left[\left[s_{f.1}^{(0)}(\boldsymbol{x}) \ldots s_{f.K}^{(0)}(\boldsymbol{x})\right]^T \left[s_{L.1}^{(0)}(\boldsymbol{x}) \ldots s_{L.K}^{(0)}(\boldsymbol{x})\right]^T\right]^T \tag{3}$$

Observe that the surrogate (3) generates predictions of the feature's coordinates. The model $\boldsymbol{s}^{(0)}(\boldsymbol{x})$ is identified using the training samples comprising vectors $\boldsymbol{x}_{Bc}^{(j)}$, $j = 1, \ldots, N_{init}$, along with the corresponding features $\boldsymbol{f}_P(\boldsymbol{x}_{Bc}^{(j)})$, assessed based on low-resolution simulations. The generation of the data points is carried out sequentially, and only the vectors of identifiable features are incorporated (see Fig. 1). The number of the initial samples N_{init} (in practice, between 50 and 200) is selected based on the required metamodel accuracy, with the parameter $E_{\max}$ (acceptance threshold for a relative RMS error) set by user. The data generation procedure is illustrated in Fig. 2. The specific number of random points allowing to acquire N_{init} decent samples is usually twice (or three times) as large as N_{init}.

ICCS Camera Ready Version 2024
To cite this paper please use the final published version:
DOI: 10.1007/978-3-031-63775-9_2

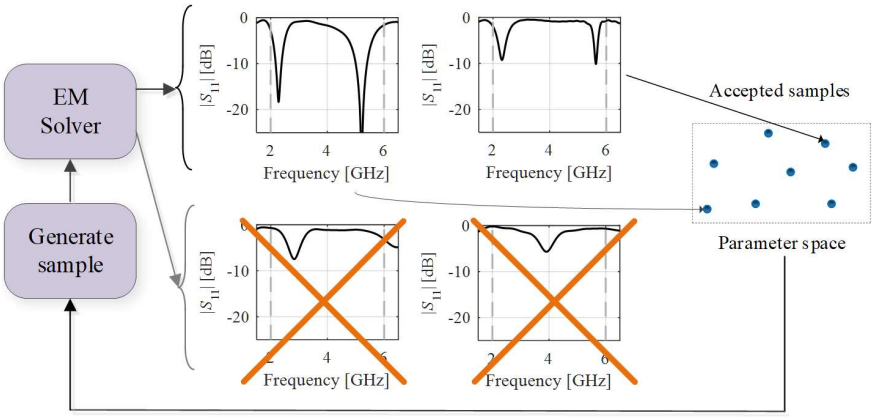

Fig. 1. Observable generation for primary model construction, which is identified using the samples whose resonances belong to the assumed target range.

1. Input parameters:
   - Design space X (interval $[\boldsymbol{l}\ \boldsymbol{u}]$, where $\boldsymbol{l}$ and $\boldsymbol{u}$ are lower and upper bounds for designable parameters; other constraints are possible per designer's needs);
   - Required modelling error E_{max};
2. Set $j = 0$;
3. Generate a sample $\boldsymbol{x}_{tmp} \in X$ using uniform probability distribution;
4. Evaluate antenna responses at $\boldsymbol{x}_{tmp}$ using low-resolution EM analysis;
5. Extract the feature vector $\boldsymbol{f}_P(\boldsymbol{x}_{tmp})$; assign $\boldsymbol{f}_P(\boldsymbol{x}_{tmp}) = 0$ if features are not extractable;
6. **if** $||\boldsymbol{f}_P(\boldsymbol{x}_{tmp})|| > 0$
   Set $j = j + 1$;
   Set $\boldsymbol{x}_{Bc}^{(j)} = \boldsymbol{x}_{tmp}$;
   Construct surrogate model $\boldsymbol{s}_{tmp}(\boldsymbol{x})$ using dataset $\{\boldsymbol{x}_{Bc}^{(k)}, \boldsymbol{f}_P(\boldsymbol{x}_B^{(k)})\}_{k=1,\ldots,j}$;
   Estimate model error E_{tmp} using K-fold cross-validation, $K = \min\{j, 10\}$;
   if $E_{tmp} < E_{max}$
   Go to 8;
   end
   end
7. Go to 3;
8. Return $\boldsymbol{s}^{(0)}(\boldsymbol{x}) = \boldsymbol{s}_{tmp}(\boldsymbol{x})$;

Fig. 2. Primary surrogate model: Training data generation.

2.6 PSO-Based Infill Points Generation. Co-Kriging Model

Once N_{init} low-fidelity data samples have been collected, the initial surrogate (3) is established. The main phase of the proposed procedure involves refinement of $\boldsymbol{s}^{(0)}(\boldsymbol{x})$ based on high-resolution data $\boldsymbol{x}_f^{(i)}$, $i = 1, 2, \ldots$, which are evaluated as

$$\boldsymbol{x}_f^{(i+1)} = \arg\min_{\boldsymbol{x} \in X} U_F(\boldsymbol{x}, \boldsymbol{s}^{(i)}(\boldsymbol{x}), \boldsymbol{F}_t) \tag{4}$$

In (4), $\boldsymbol{s}^{(j)}$, $j = 1, 2, \ldots$, refer to co-kriging models built using two datasets: (i) low-fidelity dataset $\{\boldsymbol{x}_{Bc}^{(j)}, \boldsymbol{f}_P(\boldsymbol{x}_{Bc}^{(j)})\}$, $j = 1, \ldots, N_{init}$, and (ii) high-fidelity dataset $\{\boldsymbol{x}_f^{(j)}, \boldsymbol{f}_P(\boldsymbol{x}_f^{(j)})\}$, $j = 1, \ldots, I$, which comprises the high-fidelity samples gathered up to the ith iteration.

ICCS Camera Ready Version 2024
To cite this paper please use the final published version:
DOI: 10.1007/978-3-031-63775-9_2

In current iteration, consecutive infill points are generated by globally optimizing the predictor $\boldsymbol{s}^{(i)}$ using a particle swarm optimizer (PSO) [44]. The search event terminates if: (i) successive iteration points are adequately close, i.e., $\|\boldsymbol{x}^{(i+1)} - \boldsymbol{x}^{(i)}\| < \varepsilon$, or (ii) no betterment of the merit function across the last $N_{no\_improve}$ iterations has been detected. We use the following values: $\varepsilon = 10^{-2}$ and $N_{no\_improve} = 10$.

2.7 Complete Optimization Procedure

This section provides delineation of the complete global optimization procedure. We have only three control parameters, summarized in Table 3. The discussion on parameters ε and $N_{no\_improve}$ has been already given in Section 2.6. As for the last parameter $E_{\max}$, it represents an acceptance threshold for the relative RMS error of the primary model. We use $E_{\max} = 2\%$, yet, virtually any value below ten percent may be used, because the model operates at response features. This makes functional landscape rather regular, in contrast to far more rugged landscape of entire antenna responses.

Figure 3 summarizes operating steps our algorithm. First, input data is delivered (Step 1). The algorithm is launched with the pre-screening stage (Step 2; see Section 2.5). This is followed by building the initial model (Step 3), which later on serves as a predictor for rendition of the first high-fidelity infill point (Step 5). In Steps 6 and 8, the surrogate update is performed, and the entire infill process continues until convergence.

1. Input parameters:
   - Target operating frequencies $\boldsymbol{F}_t$ (cf. Section 2.1);
   - Definition of the response features $\boldsymbol{f}_P$ and the objective function U_F (cf. Section 2.2);
   - Design space X (interval $[\boldsymbol{l}\ \boldsymbol{u}]$, where $\boldsymbol{l}$ and $\boldsymbol{u}$ are lower and upper bounds for parameters);
   - Required modelling error $E_{\max}$;
   - Termination thresholds ε and $N_{no\_improve}$;
2. Generate the set of low-resolution initial samples $\{\boldsymbol{x}_{Bc}^{(k)}, \boldsymbol{f}_P(\boldsymbol{x}_{Bc}^{(k)})\}_{k=1,\ldots,Ninit}$, (see Section 2.5),
3. Construct the initial (kriging) surrogate model $\boldsymbol{s}^{(0)}(\boldsymbol{x})$;
4. Set $i = 0$;
5. Obtain infill point $\boldsymbol{x}_f^{(i+1)}$ by solving (4) using the PSO algorithm:
$$\boldsymbol{x}_f^{(i+1)} = \arg\min_{\boldsymbol{x} \in X} U_F(\boldsymbol{x}, \boldsymbol{s}^{(i)}(\boldsymbol{x}), \boldsymbol{F}_t)$$
6. Update the dataset: $\{\boldsymbol{x}_{Bc}^{(k)}, \boldsymbol{f}_P(\boldsymbol{x}_{Bc}^{(k)})\}_{k=1,\ldots,Ninit} \cup \{\boldsymbol{x}_f^{(k)}, \boldsymbol{f}_P(\boldsymbol{x}_f^{(k)})\}_{k=1,\ldots,i}$
7. Set $i = i + 1$;
8. Construct the co-kriging surrogate model $\boldsymbol{s}^{(i)}(\boldsymbol{x})$ using the updated dataset;
9. **if** $\|\boldsymbol{x}^{(i)} - \boldsymbol{x}^{(i-1)}\| < \varepsilon$ OR no objective function improvement for $N_{no\_improve}$ iterations
   Go to 11;
   end
10. Go to 5;
11. Return $\boldsymbol{x}^* = \boldsymbol{x}_f^{(i)}$;

Fig. 3. Pseudocode of the developed global optimization framework.

Table 3. Global multi-fidelity optimization framework: Control parameters

Parameter	Meaning	Default value
$E_{\max}$	Maximum value of relative RMS error of the initial surrogate model (error estimated using cross-validation), cf. Section 2.5	2%
ε	Termination threshold for convergence in argument, cf. Section 2.6	10^{-2}
$N_{no\ improve}$	Termination threshold for no objective function value improvement, cf. Section 2.6	10

ICCS Camera Ready Version 2024
To cite this paper please use the final published version:
DOI: 10.1007/978-3-031-63775-9_2

3 Verification Case Studies

The efficacy of the developed global optimization procedure is verified in this section with the use of two antenna examples and comparisons with four state-of-the-art benchmark algorithms.

3.1 Test Cases and Experimental Setup

The introduced algorithm is applied to two microstrip antenna structures shown in Figs. 4 and 5 respectively. The same figures provide essential information about antenna substrate parameters and design variables. The EM models are realized using CST Microwave Studio [47]. The low-resolution models are obtained by reducing the discretization density of the structures (cf. Table 4). Our design goal is to relocate antenna resonant frequencies to the assumed target values. The target operating frequencies are $\boldsymbol{f}_t = [2.45\ 5.3]^T$ GHz (Antenna I) and $\boldsymbol{f}_t = [3.5\ 5.8\ 7.5]^T$ GHz (Antenna II). The lower and upper bounds for design variables are $\boldsymbol{l} = [15\ 3\ 0.35\ 0.2\ 1.8\ 0.5]^T$, $\boldsymbol{u} = [50\ 12\ 0.85\ 1.5\ 4.3\ 2.7]^T$ (Antenna I), and $\boldsymbol{l} = [10\ 17\ 0.2\ 45\ 5\ 0.4\ 0.15\ 0.2\ 0.1\ 0.5\ 0.1]^T$, $\boldsymbol{u} = [16\ 25\ 0.6\ 55\ 15\ 0.5\ 0.3\ 0.8\ 0.4\ 0.65\ 0.5]^T$ (Antenna II).

Antennas I and II were optimized using the proposed algorithm (setup: $E_{\max} = 2\%$, $\varepsilon = 10^{-2}$, $N_{no\_improve} = 10$). The benchmark algorithms have been outlined in Table 5. We have: PSO, a multiple-start gradient search, and two ML algorithms. The first one is a surrogate-based procedure with kriging metamodels, tackling complete antenna frequency characteristics. The second is akin to the feature-based algorithm proposed in Section 2 but only employs the high-resolution EM model at all search stages.

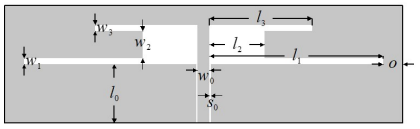

(a)

Substrate	RO4350 substrate ($\varepsilon_r = 3.48$, $h = 0.762$ mm)
Design variables	$\boldsymbol{x} = [l_1\ l_2\ l_{3r}\ w_1\ w_2\ w_3]^T$
Other variables	$l_3 = l_{3r}l_1$; $l_0 = 30$, $w_0 = 3$, $s_0 = 0.15$, $o = 5$; all dimensions except l_{3r} (which is relative) are in mm

(b)

Fig. 4. Antenna I [45]: (a) geometry, (b) essential parameters.

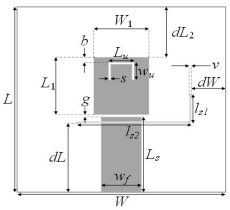

(a)

Substrate	$\varepsilon_r = 3.2$, $h = 3.06$ mm
Design variables	$\boldsymbol{x} = [L_1\ L_s\ L_{ur}\ W\ W_1\ dL_r\ dW_r\ g\ l_{s1r}\ l_{s2r}\ w_{ur}]^T$
Other variables	$b = 1$, $w_f = 7.4$, $s = 0.5$, $w = 0.5$, $dL_2 = L_1$, $L = L_s + g + L_1 + dL_2$, $L_u = L_{ur}W_1$, $dL = dL_rL$, $dW = dW_rW$, $l_{s1} = l_{s1r}(L - dL)$, $l_{s2} = l_{s2r}(W - dW)$, $w_u = w_{ur}(L_1 - b - s)$

(b)

Fig. 5. Antenna II [46]: (a) geometry, the light-shade grey indicates a ground-plane slot, (b) essential parameters.

ICCS Camera Ready Version 2024
To cite this paper please use the final published version:
DOI: 10.1007/978-3-031-63775-9_2

Table 4. Computational models for Antennas I and II

Antenna	EM simulation model			
	Low-fidelity $\boldsymbol{R}_c$		High-fidelity $\boldsymbol{R}_f$	
	Discretization density (# of mesh cells)	Simulation time [s]	Discretization density (# of mesh cells)	Simulation time [s]
I	~60,000	25	~410,000	92
II	~160,000	42	~800,000	165

Table 5. Benchmark algorithms

Algorithm	Algorithm type	Setup
I	Particle swarm optimizer (PSO)	Swarm size $N = 10$, standard control parameters ($\chi = 0.73$, $c_1 = c_2 = 2.05$); number of iterations set to 50 (version I) and 100 (version II)
II	Trust-region gradient based optimizer [48]	Random initial design, response gradients estimated using finite differentiation, termination criteria based on convergence in argument and reduction of the trust region size [48]
III	ML algorithm operating on complete antenna characteristics	Algorithm highlights: • Initial surrogate set up to ensure relative RMS error not higher than 10% with the max. number of training samples equal to 400; • Optimization based on processing the antenna frequency characteristics (unlike response features in the proposed procedure); • Infill criterion: minimization of the predicted objective function [49].
IV	Feature-based ML algorithm utilizing high-fidelity EM model only	Algorithm highlights: • Surrogate model constructed at the level of response features; • Optimization process only uses high-fidelity EM simulations; • Infill criterion: minimization of the predicted objective function [49].

3.2 Results and Discussion

Given the stochastic nature of the procedures under consideration, each algorithm has been executed ten times, and the resulting statistics are presented in Tables 6 and 7 for Antenna I and II, respectively. Figures 6 and 7 illustrate the reflection characteristics and the objective function evolution for selected runs of the algorithm. The assessment of the developed optimization procedure's performance is conducted below, taking into account factors such as the dependability of the optimization process, design quality, and cost-efficacy.

Reliability: The reliability is gauged through the success rate, representing the number of successful runs (out of ten) where the algorithm successfully positioned the antenna resonances at the intended targets. Our algorithm demonstrates a flawless success rate, comparable only to the two ML-based benchmark methods (Algorithms III and IV). Other techniques exhibit noticeable inferiority. Notably, in the case of PSO, the results highlight the significantly higher computational budget required for bio-inspired optimization.

Design Quality: Design quality is evaluated by the mean value of the cost function, which remains comparable for all algorithms. The reported differences hold minor practical importance. The seemingly poorer values displayed by Algorithms I and II result from showcasing the average performance, reduced by unsuccessful runs.

ICCS Camera Ready Version 2024
To cite this paper please use the final published version:
DOI: 10.1007/978-3-031-63775-9_2

Table 6. Optimization results for Antenna I

Optimization algorithm		Performance figure		
		Average objective function value [dB]	Computational cost[$]	Success rate[#]
Algorithm I: PSO	50 iterations	–18.2	500	9/10
	100 iterations	–19.3	1,000	10/10
Algorithm II: Trust-region gradient-based algorithm		–13.5	84.2	6/10
Algorithm III: machine learning algorithm processing complete antenna responses		–20.7	457.8	10/10
Algorithm IV: feature-based machine learning algorithm using high-fidelity EM model		–20.3	92.3	10/10
Proposed algorithm		–23.9	65.3	10/10

[$] The cost expressed in terms of the number of EM simulations of the antenna structure under design.
[#] Number of algorithms runs at which the operating frequencies were allocated in the vicinity of the target frequencies.

Table 7. Optimization results for Antenna II

Optimization algorithm		Performance figure		
		Average objective function value [dB]	Computational cost[$]	Success rate[#]
Algorithm I: PSO	50 iterations	–12.3	500	6/10
	100 iterations	–14.2	1,000	8/10
Algorithm II: Trust-region gradient-based algorithm		–12.1	125.4	4/10
Algorithm III: machine learning algorithm processing complete antenna responses		–14.2	473.0	7/10
Algorithm IV: feature-based machine learning algorithm using high-fidelity EM model		–17.9	347.0	10/10
Proposed algorithm		–15.3	89.8	10/10

[$] The cost expressed in terms of the number of EM simulations of the antenna structure under design.
[#] Number of algorithms runs at which the operating frequencies were allocated in the vicinity of the target frequencies.

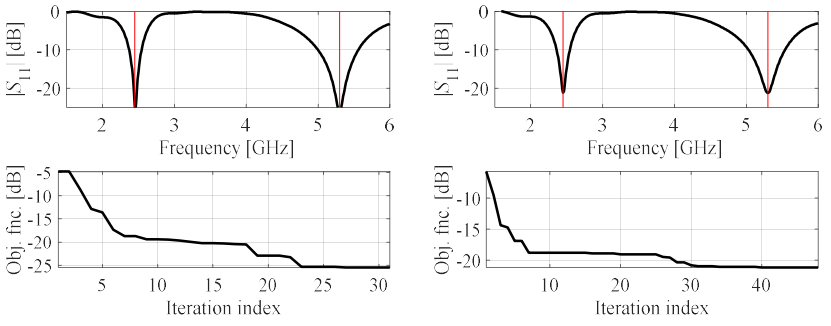

Fig. 6. $|S_{11}|$ of Antenna I evaluated for the designs generated by our algorithm (top) and evolution of the objective function value (bottom), shown for typical algorithm executions: (a) run 1, (b) run 2. The iteration counter starts upon constructing the initial surrogate model. Vertical lines represent the assumed operating frequencies, here 2.45 GHz and 5.3 GHz.

ICCS Camera Ready Version 2024
To cite this paper please use the final published version:
DOI: 10.1007/978-3-031-63775-9_2

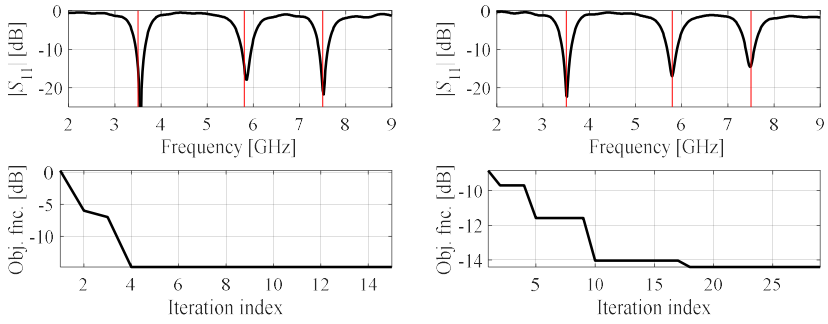

Fig. 7. $|S_{11}|$ of Antenna II evaluated for the designs generated by our algorithm (top) and evolution of the objective function value (bottom), shown for typical algorithm executions: (a) run 1, (b) run 2. The iteration counter starts after constructing the initial surrogate model. Vertical lines represent the assumed operating frequencies, here 3.5 GHz, 5.8 GHz, and 7.5 GHz.

Computational Efficiency: The proposed algorithm stands out for its lower running cost compared to other global search algorithms. The average expenses, assessed as the equivalent number of high-resolution EM simulations, are only 65 and 90 for Antenna I and II, respectively. This implies a cost reduction of 30% and 74% for Antenna I and II compared to Algorithm IV (similar to the proposed one but using the high-fidelity model only). It is noteworthy that the computational benefits increase with problem complexity. The majority of antenna evaluations occur in the initial stage of the search procedure (parameter space pre-screening and initial surrogate model rendition) with the use of the low-fidelity model. Another observation is that the proposed algorithm only required 77 and 259 random observables in the first stage of the optimization process for Antennas I and II (in both cases, achieving the modeling error $E_{\max}$). Conversely, Algorithm III, working with complete antenna responses, could not reach the required accuracy limit, necessitating the establishment of the surrogate using 400 data samples (the allowed budget). Thus, leveraging response features leads to a notable reduction in computational expenses during this stage of the process.

This analysis suggests that the proposed algorithm serves as a viable alternative to existing global search techniques. Although demonstrated for multi-band antennas, comparable performance is anticipated for other problem types, provided they can be reformulated using response features. The primary advantages of our technique lie in reliability, computational efficiency, and a straightforward setup: with only three control parameters, two of which relate to termination criteria.

4 Conclusion

This study has introduced an innovative approach to achieving low-cost global optimization for antenna structures. Our methodology capitalizes on the characteristics of response features, employing a feature-based reformulation to serve as a tool for regularization of the optimization task. The search process is structured within a machine learning (ML) framework, utilizing kriging interpolation surrogates as the primary predictor. This surrogate is employed to generate promising candidate solutions (infill

ICCS Camera Ready Version 2024
To cite this paper please use the final published version:
DOI: 10.1007/978-3-031-63775-9_2

points), with iterative refinement using accumulated electromagnetic (EM) simulation data. The involvement of multi-fidelity EM simulations is instrumental in reducing the algorithm's running cost. Specifically, initial parameter space sampling and surrogate model construction are executed using low-fidelity EM simulations, while the ML process leverages high-fidelity EM analysis, seamlessly blended with the low-fidelity samples through co-kriging. Our methodology has undergone comprehensive validation using two microstrip antennas, demonstrating exceptional computational efficiency (with an average cost not exceeding ninety high-fidelity EM simulations per run), result consistency, and a significant speedup compared to benchmark methods. These benchmarks encompass both nature-inspired and ML routines.

Acknowledgement

The authors would like to thank Dassault Systemes, France, for making CST Microwave Studio available. This work is partially supported by the Icelandic Centre for Research (RANNIS) Grant 239858 and by National Science Centre of Poland Grant 2022/47/B/ST7/00072.

References

1. Yuan, X.-T., Chen, Z., Gu, T., Yuan T.: A wideband PIFA-pair-based MIMO antenna for 5G smartphones. IEEE Ant. Wireless Propag. Lett., **20**, pp. 371–375 (2021)
2. Sun, L., Li, Y., Zhang Z.: Wideband decoupling of integrated slot antenna pairs for 5G smartphones. IEEE Trans. Ant. Prop., **69**, pp. 2386–2391 (2021)
3. Kapusuz, K.Y., Berghe, A.V., Lemey, S., Rogier H.: Partially filled half-mode substrate integrated waveguide leaky-wave antenna for 24 GHz automotive radar. IEEE Ant. Wireless Propag. Lett., 20, pp. 33–37 (2021)
4. Ameen, M., Thummaluru, S.R., Chaudhary R.K.: A compact multilayer triple-band circularly polarized antenna using anisotropic polarization converter. IEEE Ant. Wireless Propag. Lett., **20**, pp. 145–149 (2021)
5. Aqlan, B., Himdi, M., Vettikalladi, H., Le-Coq L.: A circularly polarized sub-terahertz antenna with low-profile and high-gain for 6G wireless communication systems. IEEE Access, **9**, pp. 122607–122617 (2021)
6. Wen, Z.-Y., Ban, Y.-L., Yang, Y., Wen Q.: Risley-prism-based dual-circularly polarized 2-D beam scanning antenna with flat scanning gain. IEEE Ant. Wireless Propag. Lett., **20**, pp. 2412–2416 (2021)
7. Shirazi, M., Li, T., Huang, J., Gong X.: A reconfigurable dual-polarization slot-ring antenna element with wide bandwidth for array applications. IEEE Trans. Ant. Prop., **66**, pp. 5943–5954 (2018)
8. Chen, C.: A compact wideband endfire filtering antenna inspired by a uniplanar microstrip antenna. IEEE Ant. Wireless Propag. Lett., **21**, pp. 853–857 (2022)
9. Wu, Y.F., Cheng, Y.J., Zhong, Y.C., Yang H.N.: Substrate integrated waveguide slot array antenna to generate Bessel beam with high transverse linear polarization purity. IEEE Trans. Ant. Propag., **70**, pp. 750–755 (2022)
10. Lee, J., Kim, H., Oh J.: Large-aperture metamaterial lens antenna for multi-layer MIMO transmission for 6G. IEEE Access, **10**, pp. 20486–20495 (2022)

ICCS Camera Ready Version 2024
To cite this paper please use the final published version:
DOI: 10.1007/978-3-031-63775-9_2

11. Chen, Z.Zhang, H.C., Cheng, Q.S.: Surrogate-assisted quasi-Newton enhanced global optimization of antennas based on a heuristic hypersphere sampling. IEEE Trans. Ant. Propag., **69**, pp. 2993–2998 (2021)
12. Nocedal, J., Wrigth, S.J., Numerical Optimization, 2nd Ed., Springer, New York (2006)
13. Conn, A.R., Scheinberg, K., Vicente, L.N., Derivative-Free Optimization. MPS-SIAM Series on Optimization, Society for Industrial and Applied Mathematics, Philadelphia (2009
14. Xu, Y., Song, Y., Pi, D., Chen, Y., Qin, S., Zhang, X., Yang, A.: A reinforcement learning-based multi-objective optimization in an interval and dynamic environment. Knowledge-Based Syst., **280**, paper No. 111019 (2023)
15. Zhu, D.Z., Werner, P.L., Werner D.H.: Design and optimization of 3-D frequency-selective surfaces based on a multiobjective lazy ant colony optimization algorithm. IEEE Trans. Ant. Propag., **65**, pp. 7137–7149 (2017)
16. Du, J., Roblin, C.: Stochastic surrogate models of deformable antennas based on vector spherical harmonics and polynomial chaos expansions: application to textile antennas. IEEE Trans. Ant. Prop., **66**, pp. 3610–3622 (2018)
17. Blankrot, B., Heitzinger, C.: Efficient computational design and optimization of dielectric metamaterial structures. IEEE J. Multiscale Multiphysics Comp. Techn., **4**, pp. 234–244 (2019)
18. Qian, B., Huang, X., Chen, X., Abdullah, M., Zhao, L., Kishk A.A.: Surrogate-assisted defected ground structure design for reducing mutual coupling in 2 × 2 microstrip antenna array. IEEE Ant. Wireless Propag. Lett., **21**, pp. 351–355 (2022)
19. Koziel, S., Pietrenko-Dabrowska, A., : Reliable EM-driven size reduction of antenna structures by means of adaptive penalty factors. IEEE Trans. Ant. Propag., **70**, pp. 1389–1401 (2021)
20. Li, W., Zhang, Y., Shi X.: Advanced fruit fly optimization algorithm and its application to irregular subarray phased array antenna synthesis. IEEE Access, **7**, pp. 165583–165596 (2019)
21. Jia, X., Lu, G.: A hybrid Taguchi binary particle swarm optimization for antenna designs. IEEE Ant. Wireless Propag. Lett., **18**, pp. 1581–1585 (2019)
22. Ding, D., Wang, G.: Modified multiobjective evolutionary algorithm based on decomposition for antenna design. IEEE Trans. Ant. Propag., **61**, pp. 5301–5307 (2013)
23. Zhang, H., Bai, B., Zheng, J., Zhou Y.: Optimal design of sparse array for ultrasonic total focusing method by binary particle swarm optimization. IEEE Access, **8**, pp. 111945–111953 (2020)
24. Michalewicz, Z.: Genetic algorithms + data structures = evolution programs, Springer, New York, (1996)
25. Wang, D., Tan, D., Liu L.: Particle swarm optimization algorithm: an overview. Soft Computing, **22**, pp. 387–408 (2018)
26. Jiang, Z.J., Zhao, S., Chen, Y., Cui T.J.: Beamforming optimization for time-modulated circular-aperture grid array with DE algorithm. IEEE Ant. Wireless Propag. Lett., **17**, pp. 2434–2438 (2018)
27. Baumgartner, P., Baurnfeind, T., Biro, O., Hackl, A., Magele, C., Renhart, W., Torchio R.: Multi-objective optimization of Yagi-Uda antenna applying enhanced firefly algorithm with adaptive cost function. IEEE Trans. Magnetics, **54**, article no. 8000504 (2018)
28. Mostafa, R.R., Gaheen, M.A., El-Aziz, M.A., Al-Betar, Ewees, A.A.:An improved gorilla troops optimizer for global optimizatio problems A.A.: . Knowledge-Based Syst., 269, paper No. 110462 (2023)
29. Ram, G., Mandal, D., Kar, R., Ghoshal S.P.: Cat swarm optimization as applied to time-modulated concentric circular antenna array: analysis and comparison with other stochastic optimization methods. IEEE Trans. Antennas Propag., **63**, pp. 4180–4183 (2015)

ICCS Camera Ready Version 2024
To cite this paper please use the final published version:
DOI: 10.1007/978-3-031-63775-9_2

30. Easum, J.A., Nagar, J., Werner, P.L., Werner D.H.: Efficient multi-objective antenna optimization with tolerance analysis through the use of surrogate models. IEEE Trans. Ant. Prop., **66**, pp. 6706–6715 (2018)
31. Jones, D.R., Schonlau, M., Welch W.J.: Efficient global optimization of expensive black-box functions. J. Global Opt., **13**, pp. 455–492 (1998)
32. Chen, C., Liu, J., Xu P.: Comparison of infill sampling criteria based on Kriging surrogate model. Sc. Rep., **12**, Art. No. 678 (2022)
33. De Villiers, D.I.L., Couckuyt, I., Dhaene T.: Multi-objective optimization of reflector antennas using kriging and probability of improvement. Int. Symp. Ant. Prop., pp. 985-986, San Diego, USA (2017)
34. Qin, J., Dong, W., Wang, M.: Fast multi-objective optimization of multi-parameter antenna structures based on improved BPNN surrogate model. IEEE Access, **7**, pp. 77692–77701 (2019)
35. Hu, C., Zeng, S., Li C.: A framework of global exploration and local exploitation using surrogates for expensive optimization. Knowledge-Based Syst., **280**, paper No. 111018 (2023)
36. Xiao, S., Liu, G.Q., Zhang, K.L., Jing, Y.Z., Duan, J.H., Di Barba, P., Sykulski J.K.: Multi-objective Pareto optimization of electromagnetic devices exploiting kriging with Lipschitzian optimized expected improvement. IEEE Trans. Magn., **54**, paper No. 7001704 (2018)
37. Koziel, S., Pietrenko-Dabrowska, A., Performance-driven surrogate modeling of high-frequency structures. Springer, New York (2020)
38. Pietrenko-Dabrowska, A., Koziel, S.: Antenna modeling using variable-fidelity EM simulations and constrained co-kriging. IEEE Access, **8**, pp. 91048–91056 (2020)
39. Pietrenko-Dabrowska, A., Koziel, S.: Generalized formulation of response features for reliable optimization of antenna input characteristics. IEEE Trans. Ant. Propag., **70**, pp. 3733–3748 (2021)
40. Pietrenko-Dabrowska, A., Koziel, S.: Simulation-driven antenna modeling by means of response features and confined domains of reduced dimensionality. IEEE Access, **8**, pp. 228942–228954 (2020)
41. Pietrenko-Dabrowska, A., Koziel, S., Ullah U.: Reduced-cost two-level surrogate antenna modeling using domain confinement and response features. Sc. Rep., **12**, Art. No. 4667 (2022)
42. Koziel, S. Fast simulation-driven antenna design using response-feature surrogates. Int. J. RF & Micr. CAE, **25**, pp. 394–402 (2015)
43. Kennedy, M.C. O'Hagan, A. Predicting the output from complex computer code when fast approximations are available. Biometrika, **87**, pp. 1–13 (2000)
44. Vinod Chandra. S.S., Anand, H.S. Nature inspired meta heuristic algorithms for optimization problems. Computing, **104**, pp. 251–269 (2022)
45. Chen, Y.-C., Chen, S.-Y., Hsu, P.: Dual-band slot dipole antenna fed by a coplanar waveguide. Proc. IEEE Antennas Propag. Soc. Int. Symp., Albuquerque, NM, USA, pp. 3589–3592 (2006)
46. Consul, P.: Triple band gap coupled microstrip U-slotted patch antenna using L-slot DGS for wireless applications. Communication, Control and Intelligent Systems (CCIS), Mathura, India, pp. 31-34 (2015)
47. CST Microwave Studio, ver. 2021, Dassault Systemes, France (2021)
48. Conn, A.R., Gould, N.I.M., Toint, P.L.: Trust Region Methods, MPS-SIAM Series on Optimization (2000)
49. Liu, J., Han, Z., Song, W.: Comparison of infill sampling criteria in kriging-based aerodynamic optimization. 28th Int. Congress of the Aeronautical Sciences, pp. 1-10, Brisbane, Australia, 23-28 Sept. (2012)

ICCS Camera Ready Version 2024
To cite this paper please use the final published version:
DOI: 10.1007/978-3-031-63775-9_2